CANCER

ARID1A mutation plus CXCL13 expression act as combinatorial biomarkers to predict responses to immune checkpoint therapy in mUCC

Sangeeta Goswami[1], Yulong Chen[1], Swetha Anandhan[1], Peter M. Szabo[2], Sreyashi Basu[3], Jorge M. Blando[3]*, Wenbin Liu[3], Jan Zhang[1], Seanu Meena Natarajan[1], Liangwen Xiong[1], Baoxiang Guan[1], Shalini Singh Yadav[3], Abdel Saci[2], James P. Allison[3,4], Matthew D. Galsky[5], Padmanee Sharma[1,3,4†]

Immune checkpoint therapy (ICT) can produce durable antitumor responses in metastatic urothelial carcinoma (mUCC); however, the responses are not universal. Despite multiple approvals of ICT in mUCC, we lack predictive biomarkers to guide patient selection. The identification of biomarkers may require interrogation of both the tumor mutational status and the immune microenvironment. Through multi-platform immuno-genomic analyses of baseline tumor tissues, we identified the mutation of AT-rich interactive domain-containing protein 1A (*ARID1A*) in tumor cells and expression of immune cytokine CXCL13 in the baseline tumor tissues as two predictors of clinical responses in a discovery cohort ($n = 31$). Further, reverse translational studies revealed that CXCL13$^{-/-}$ tumor-bearing mice were resistant to ICT, whereas *ARID1A* knockdown enhanced sensitivity to ICT in a murine model of bladder cancer. Next, we tested the clinical relevance of *ARID1A* mutation and baseline CXCL13 expression in two independent confirmatory cohorts (CheckMate275 and IMvigor210). We found that *ARID1A* mutation and expression of CXCL13 in the baseline tumor tissues correlated with improved overall survival (OS) in both confirmatory cohorts (CheckMate275, CXCL13 data, $n = 217$; ARID1A data, $n = 139$, and IMvigor210, CXCL13 data, $n = 348$; ARID1A data, $n = 275$). We then interrogated CXCL13 expression plus *ARID1A* mutation as a combination biomarker in predicting response to ICT in CheckMate275 and IMvigor210. Combination of the two biomarkers in baseline tumor tissues suggested improved OS compared to either single biomarker. Cumulatively, this study revealed that the combination of CXCL13 plus ARID1A may improve prediction capability for patients receiving ICT.

INTRODUCTION

Urothelial cancer is the sixth most common cancer in the United States and makes up about 5% of new cancer cases each year (*1*). The 5-year overall survival (OS) rate in metastatic urothelial cancer (mUCC) is around 5% (www.cancer.org). Approval of immune checkpoint therapies (ICTs) for treatment of mUCC represented a paradigm shift because it demonstrated durable responses and improved OS (*2*–*9*). Despite durable antitumor responses and multiple approvals, responses are not universal, and we lack predictive biomarkers to guide treatment decisions (*10*, *11*). Therefore, there is a critical need to develop clinically useful biomarkers to refine patient selection.

Notable efforts have been made for development of predictive biomarkers for patients with mUCC receiving ICT (*12*). A major focus was on developing programmed death-ligand 1 (PD-L1) as a predictive biomarker; however, data from clinical trials varied markedly, highlighting the difficulty of using PD-L1 as a single biomarker (*13*). In addition to technical issues such as standardization of PD-L1 assays, dynamic regulation of PD-L1 expression in the tumor microenvironment may explain lack of reproducibility of PD-L1 as a single biomarker. Similarly, tumor mutation burden (TMB), The Cancer Genome Atlas (TCGA) subtyping, and gene expression profiling (GEP) as single biomarkers were unable to differentiate patients with mUCC who would respond to ICT (*11*, *14*). The single biomarker studies focused on either tumor mutations or immune response biomarkers, which may limit predictive power because of the lack of integration between cancer cell biology and immune cell responses.

To address this need, we interrogated both the immune microenvironment and the tumor mutational profile to identify a potential combinatorial biomarker to predict response to ICT. For the discovery cohort, patient samples were obtained at MD Anderson Cancer Center from two clinical trials: a phase 2 study assessing the safety and efficacy of nivolumab in metastatic or surgically unresectable urothelial carcinoma that progressed or recurred despite previous treatment with at least one platinum-based chemotherapy regimen (NCT02387996) and a phase 1/2, open-label study of nivolumab monotherapy or nivolumab combined with ipilimumab in subjects with advanced or metastatic solid tumors (NCT01928394) (*15*). Responders were defined as complete responses (CRs) and partial responses (PRs) as per RECIST (Response Evaluation Criteria in Solid Tumors) v1.1 and included patients with stable disease (SD) greater than or equal to 6 months, whereas nonresponders were defined as patients with progressive disease (PD). We used CheckMate275 biomarker cohort (*5*) and IMvigor210 (*4*, *16*) as our two independent confirmatory cohorts.

[1]Department of Genitourinary Medical Oncology, The University of Texas MD Anderson Cancer Center, Houston, TX 77030, USA. [2]Department of Translational Medicine, Bristol Myers Squibb, Princeton, NJ 08540, USA. [3]Immunotherapy Platform, The University of Texas MD Anderson Cancer Center, Houston, TX 77030, USA. [4]Department of Immunology, The University of Texas MD Anderson Cancer Center, Houston, TX 77030, USA. [5]Division of Hematology and Medical Oncology, Department of Medicine, Icahn School of Medicine at Mount Sinai/Tisch Cancer Institute, New York, NY 10029, USA.
*Present address: AstraZeneca, Gaithersburg, MD 20878, USA.
†Corresponding author. Email: padsharma@mdanderson.org

We identified the expression of immune cytokine CXCL13 in the baseline tumor tissues and *ARID1A* mutation in tumor cells as predictors of clinical responses to ICT in patients with mUCC in the discovery cohort ($n = 31$). Further, reverse translational studies revealed that CXCL13$^{-/-}$ tumor-bearing mice were resistant to ICT, whereas *ARID1A* knockdown enhanced sensitivity to ICT in a murine model of bladder cancer. Next, we tested the clinical relevance of baseline CXCL13 expression and *ARID1A* mutation in two independent confirmatory cohorts (CheckMate275 and IMvigor210). We found that *ARID1A* mutation and expression of CXCL13 in the baseline tumor tissues correlated with improved response and OS in both confirmatory cohorts (CheckMate275 and IMvigor210). Next, we interrogated CXCL13 expression plus *ARID1A* mutation as a combinatorial biomarker in predicting response to ICT in CheckMate275 and IMvigor210. Combination of both biomarkers in baseline tumor tissues suggested improved OS compared to either single biomarker. Cumulatively, this study revealed that the combination biomarkers of CXCL13 plus ARID1A may improve predictive outcomes for patients receiving ICT and enable patient selection for ICT.

RESULTS

ARID1A mutation correlates with improved OS in patients with mUCC receiving ICT

Whole-exome sequencing from paired baseline bladder tumor samples and peripheral blood mononuclear cells (PBMCs) (as controls) was performed to identify tumor-specific mutations ($n = 24$). Patient characteristics of the discovery cohort are described in data file S1. We selected the most mutated genes from the TCGA bladder cancer cohort (*17*) (www.cbioportal.org) and ordered by decreasing frequency of occurrence in the clinical cohort (Fig. 1A). *ARID1A* was the only gene mutation in our discovery cohort that was significantly enriched in responders as compared to nonresponders ($P = 0.03$). Specifically, a total of four patients' tumors harbored *ARID1A* mutations (missense, $n = 2$; nonsense, $n = 1$; and splice site mutations, $n = 1$) among the 11 responders, whereas no *ARID1A* mutations were noted in tumors of nonresponders (Fig. 1A). In addition, we noted that *ARID1A* mutations resulted in the down-regulation of *ARID1A* expression (Fig. 1B).

ARID1A is a subunit of switch/sucrose nonfermentable (SWI/SNF) complex required for chromatin remodeling and known to interact with the transcription machinery (*18*). Previously published preclinical data using cell lines and a murine ovarian tumor model showed that knockdown of *ARID1A* in ovarian tumor cell lines (ID8) increased sensitivity to ICT (*19*). Similarly, we noted that knockdown of *ARID1A* in MB49 bladder cancer cell line increased sensitivity to anti–PD-1 therapy in tumor-bearing mice (fig. S2A). Further, RNA sequencing (RNA-seq) and gene set enrichment analysis (GSEA) of control (scramble) and *ARID1A*-knockdown MB49 cell lines showed that loss of *ARID1A* altered the expression of distinct pathways regulating immune responses in the tumor. *ARID1A* knockdown up-regulated interferon response genes and cytokine pathways in the tumor cells (fig. S2, B and C), whereas the DNA repair and angiogenesis pathways were down-regulated (fig. S2C). Cumulatively, these data suggested that loss of *ARID1A* could enhance the immunogenicity of bladder tumor cells.

Next, we tested the clinical relevance of *ARID1A* mutation in patients with mUCC receiving ICT in two independent confirmatory cohorts (CheckMate275 and IMvigor210). The Consolidated Standards of Reporting Trials (CONSORT) diagram described the number of samples used to analyze genomic and other correlates in each of the confirmatory cohorts (fig. S1, A and B). Consistent with a previous report (*19*), we found that patients harboring *ARID1A* gene mutation have higher TMB compared to patients without the mutation in both the confirmatory cohorts and the TCGA cohort (fig. S3, A to C). However, hazard curve analysis of TMB by *ARID1A* mutation status showed that patients with higher TMB plus *ARID1A* mutation had improved progression-free survival (PFS) and OS compared to patients with higher TMB but without the *ARID1A* mutations (fig. S3D), suggesting that ARID1A might modulate tumor immune microenvironment through multiple pathways. In IMvigor210, it was shown that transforming growth factor β1 (TGFβ1) attenuates response to anti–PD-L1 therapy in patients with mUCC (*16*). Therefore, we tested whether *ARID1A* mutation correlates with TGFβ1 expression. We noted that TGFβ1 expression was significantly lower in patients harboring *ARID1A* gene mutation compared to patients without the mutation, in IMvigor210 cohort ($^*P < 0.05$) as well as in TCGA cohort ($^{**}P < 0.01$) (fig. S4, A and B). We did not see any difference in PD-L1 expression in tumor or in immune cells based on the presence or absence of *ARID1A* mutation in discovery and confirmatory (CheckMate275 and IMvigor210) cohorts (fig. S4, C to E). Next, we compared the responses in patients with and without *ARID1A* mutation. Similar to discovery cohort, *ARID1A* mutations correlated with improved clinical outcome and responses (CR/PR/SD $\geq$ 6 months) as compared to patients without *ARID1A* mutations in confirmatory cohorts (CheckMate275 and IMvigor210) (Fig. 1, C and D). Because of sample sizes, we could not estimate OS in the discovery cohort. Therefore, we assessed association of *ARID1A* mutation with OS in our confirmatory cohorts. We observed a significant association between *ARID1A* mutation and OS in CheckMate275 ($n = 139$) ($P = 0.03$) and IMvigor210 ($n = 275$) ($P = 0.03$) (Fig. 1, E and F). In the CheckMate275 cohort ($n = 139$), we noted median OS of 11.4 months [95% CI confidence interval (CI), 5.48 to not attained (NA)] in patients with *ARID1A* mutation, whereas median OS was 6.0 months (95% CI, 4.6 to 11.3) in patients without *ARID1A* mutation, demonstrating a significant association of *ARID1A* mutation and OS ($P = 0.03$) (Fig. 1E). In the IMvigor210 cohort ($n = 275$), we noted median OS of 15.4 months (95% CI, 9.2 to NA) in patients with *ARID1A* mutation, whereas median OS was 8.2 months (95% CI, 6.7 to 10.9) in patients without *ARID1A* mutation, also demonstrating a significant association of *ARID1A* mutation and OS ($P = 0.03$) (Fig. 1F). Together, we identified *ARID1A* mutation in the baseline bladder tumor tissue to be predictive of favorable responses to ICT in patients with mUCC.

Expression of CXCL13 in baseline tumor tissues correlates with improved OS

To integrate the genomic and immunological determinants of clinical responses to ICT in mUCC, we sought to identify an immunological biomarker that can predict response to ICT. To profile the immune subpopulations, we performed immunohistochemistry (IHC) analysis on the baseline bladder tumor samples in the discovery cohort ($n = 31$). We noted predominant intratumoral infiltration of CD4$^+$ and CD8$^+$ T lymphocytes and CD20$^+$ B cells in responders (11) compared to nonresponders (20) (Fig. 2A). As recently published for other tumor types (*20*–*22*), we also noted an increased density of tertiary lymphoid structures (TLSs) in the baseline tumor tissues of responders compared to nonresponders in patients with mUCC

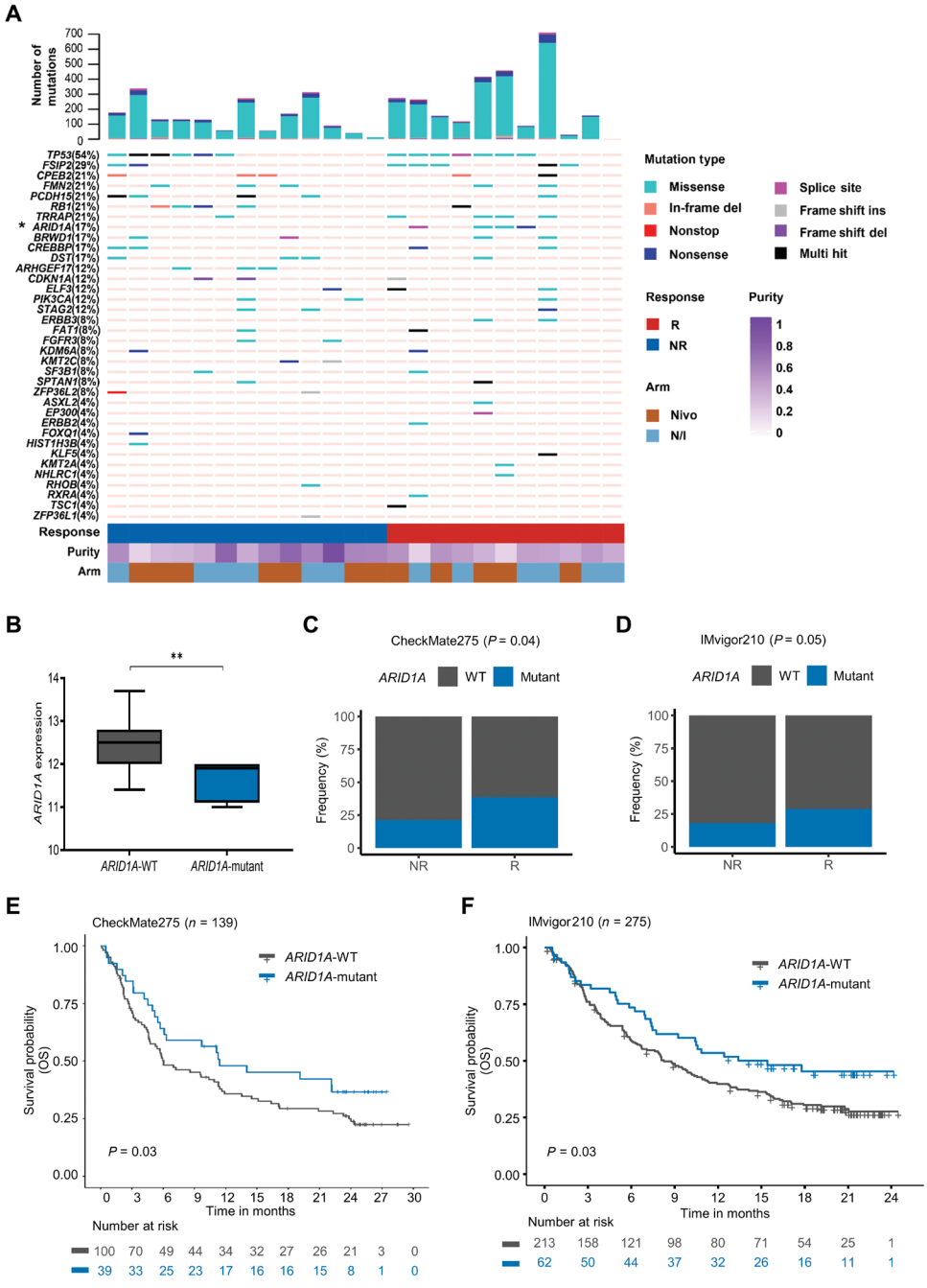

Fig. 1. *ARID1A* mutation in the baseline bladder tumor tissue correlates with favorable responses to ICT. (**A**) An "oncoplot" showing the 34 commonly mutated genes in bladder cancer. Each column represents a patient tumor sample, and each row represents a different gene. The numbers on the left side represent the percentages of mUCC samples carrying mutations in each specific gene. The top barplot indicates the frequency of mutations for each patient. *ARID1A* is the only gene that has significantly higher mutation frequency in the responders (R) group ($n = 11$) than in the nonresponder (NR) group ($n = 13$) (*$P = 0.031$, Fisher's exact test). (**B**) Representative plot of *ARID1A* gene expression in patients with no *ARID1A* mutation (*ARID1A*-WT) ($n = 20$) and with *ARID1A* mutation (*ARID1A* mutant) ($n = 4$). **$P < 0.01$. (**C**) Stack bar plot showing the frequencies of patients with no *ARID1A* mutation (WT) and with *ARID1A* mutation (mutant) in the R group ($n = 57$) and in the NR group ($n = 61$) in the CheckMate275 trial. *P* value from logistic regression with response groups (R versus NR) as the dependent variable and *ARID1A* mutation status as the independent variable. (**D**) Stack bar plot showing the frequencies of patients with no *ARID1A* mutation (WT) and with *ARID1A* mutation (mutant) in the R group ($n = 104$) and in the NR group ($n = 133$) in the IMvigor210 trial. *P* value from logistic regression with response groups (R versus NR) as the dependent variable and *ARID1A* mutation status as the independent variable. (**E**) Kaplan-Meier plot showing overall survival (OS) ($P = 0.03$) in patients with mUCC divided into *ARID1A*-WT (those with no *ARID1A* mutation) and *ARID1A*-mutant (those with *ARID1A* mutation) ($n = 139$, *ARID1A*-WT = 100, *ARID1A*-mutant = 39) in the CheckMate275 trial. (**F**) Kaplan-Meier plot showing OS ($P = 0.03$) in patients with mUCC divided into *ARID1A*-WT (those with no *ARID1A* mutation) and *ARID1A*-mutant (those with *ARID1A* mutation) ($n = 275$, *ARID1A*-WT = 213, *ARID1A*-mutant = 62) in the IMvigor210 trial.

(fig. S5, A to C). To identify genes in the baseline bladder tumor specimens of responders (R = 8) and nonresponders (NR = 13) that may correlate with differential immune infiltration and TLS, we performed targeted gene expression analysis via a custom 739-gene NanoString panel (data file S2). We identified genes implicated in immune infiltration and TLSs (*23*), which included CXCL13, CXCL9, CCL19, and CCL5 (Fig. 2B and fig. S5D). Whereas CXCL9, CCL19, and CCL5 play a role in T cell infiltration, CXCL13 plays a critical role in both T and B cell infiltration (*24*). Therefore, we chose to focus on CXCL13 as a potential immunologic biomarker for correlation with responses to ICT.

To test the role of CXCL13 in ICT-mediated antitumor immunity in bladder cancer, we used CXCL13 null ($CXCL13^{-/-}$) mice bearing murine bladder tumors (MB49). We treated wild-type (WT) and $CXCL13^{-/-}$ MB49 tumor-bearing mice with anti–PD-1 therapy. Whereas WT-MB49 tumor-bearing mice responded to anti–PD-1 therapy, $CXCL13^{-/-}$ mice did not respond to anti–PD-1 treatment (fig. S6A). In addition, we observed lower frequency of T cell infiltration in $CXCL13^{-/-}$ tumor-bearing mice as compared to WT tumor-bearing mice (fig. S6B). Further, $CXCL13^{-/-}$ tumor-bearing mice failed to have an increase in tumor-infiltrating T cells after treatment with anti–PD-1 as compared to WT mice (fig. S6B). Together, the murine studies provided evidence for direct association between CXCL13 and anti–PD-1–mediated antitumor immunity.

Next, we tested the significance of CXCL13 as an immunological biomarker in our confirmatory cohorts (CheckMate275 and IMvigor210). We saw higher expression of CXCL13 in the responders as compared

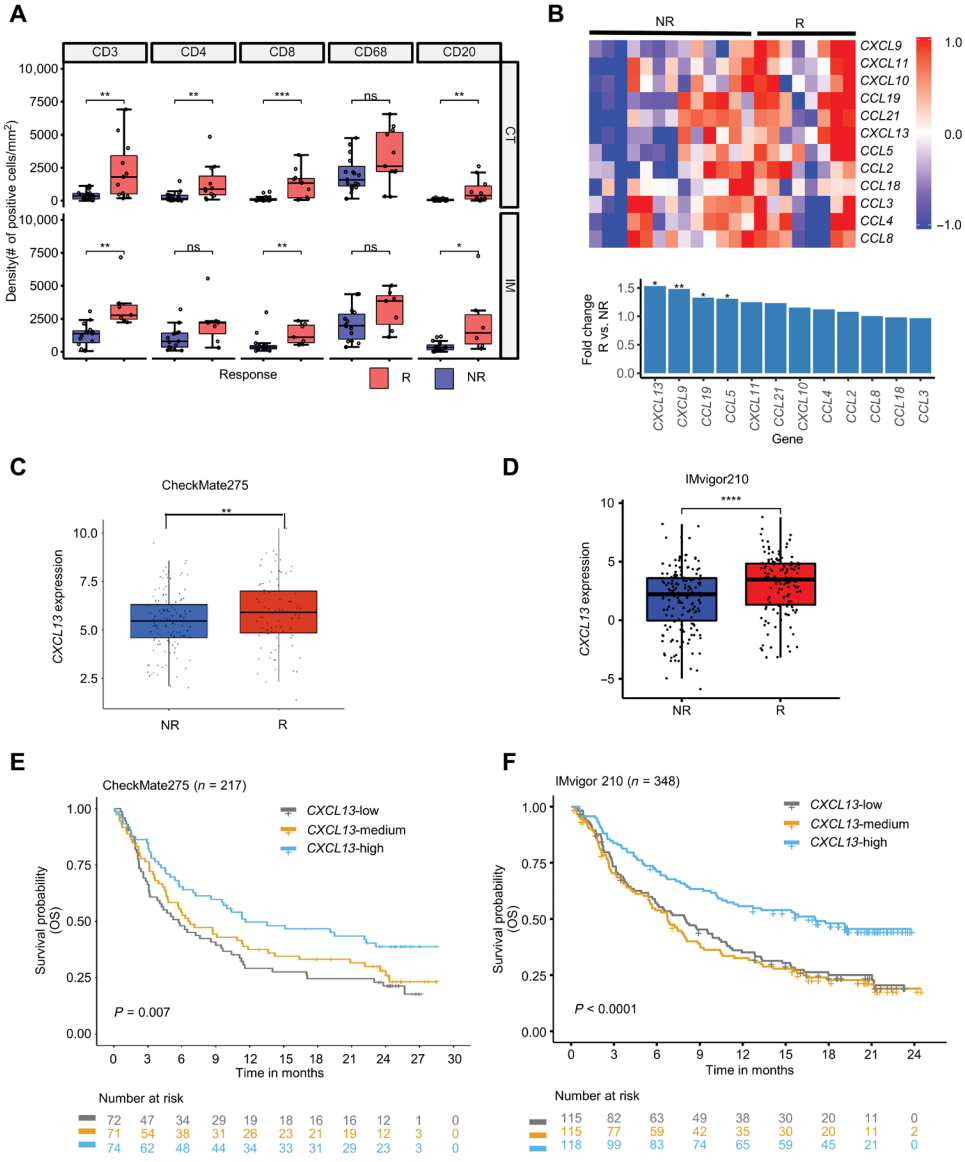

Fig. 2. High baseline CXCL13 expression in tumor tissues confers sensitivity to ICT. (**A**) Quantification of expression of indicated markers via IHC analysis on patient tumor samples ($n = 31$) with R = 11 and NR = 20. IM, margin; CT, center. (**B**) Top: Representative heat map of the 12 TLS signature genes using GEP of baseline mUCC tumor specimens ($n = 21$; R = 8, NR = 13) using customized 739-gene NanoString panel. Bottom: Bar graph showing the fold difference of 12 TLS signature genes between R and NR baseline mUCC tumor specimens. Bars are ordered by fold change. *$P < 0.05$, **$P < 0.01$. (**C**) Representative box plot of *CXCL13* gene expression in patients in the R group and in the NR group in the CheckMate275 trial. **$P < 0.01$. (**D**) Representative box plot of *CXCL13* gene expression in patients in the R group ($n = 104$) and in the NR group ($n = 133$) in the IMvigor210 trial. ****$P < 0.0001$. (**E**) Kaplan-Meier estimates of OS in patients in the CheckMate275 trial, stratified according to the 33rd and 66th percentile of *CXCL13* expression values ($P = 0.007$). (**F**) Kaplan-Meier estimates of OS in patients in the IMvigor210 trial, stratified according to the 33rd and 66th percentile of *CXCL13* expression values ($P < 0.0001$).

to nonresponders in both CheckMate275 ($n = 118$) ($P < 0.01$) and IMvigor210 ($n = 237$) ($P < 0.0001$) (Fig. 2, C and D). Next, we divided the cohort of bladder cancer patients into high, medium, and low expression of CXCL13 based on tertiles. We observed that higher expression of CXCL13 correlated with improved OS ($P = 0.007$) in CheckMate275 (Fig. 2E). We noted median OS of 13.5 months (95% CI, 7.22 to NA) in the CXCL13-high cohort, 6.6 months (95% CI, 4.6 to 11.4) in the CXCL13-medium cohort, and 5.7 (95% CI, 3.15 to 9.49) months in the CXCL13-low cohort. We also noted a significant association between higher CXCL13 expression and OS ($P < 0.0001$) in IMvigor210 (Fig. 2F). We noted median OS of 17.1 months (95% CI, 10.9 to NA) in the CXCL13-high cohort, 6.7 months (95% CI, 5.5 to 8.8) in the CXCL13-medium cohort, and 8.0 months (95% CI, 5.8 to 10.8) in the CXCL13-low cohort. Together, we identified CXCL13 expression in pretreatment tumor tissue as an immunologic biomarker of favorable responses to ICT in patients with mUCC.

Combination of *ARID1A* mutation and baseline expression of CXCL13 in the tumor tissue predicts performance to ICT

In the confirmatory cohorts, both *ARID1A* mutation and higher CXCL13 expression in the baseline tumor samples were independently associated with improved OS. Further, reverse translational studies provided evidence of direct association of CXCL13 expression and *ARID1A* mutation with anti–PD-1–mediated antitumor immunity. However, based on previous biomarker studies, we have learned that single genomic or immunological biomarker could not reproducibly predict responses to ICT because of dynamic interactions between tumor cells and immune cells. Therefore, we tested whether combination of *ARID1A* mutation and CXCL13 expression have improved predictive capacity compared to either single biomarker. In CheckMate275, we observed a median PFS of 3.7 months (95% CI, 1.8 to NA) in patients with *ARID1A* mutation and high CXCL13, 1.7 months (95% CI, 0.8 to 5.5) in patients with *ARID1A* mutation and low CXCL13, 1.9 months (95% CI, 1.7 to 3.2) in patients with no *ARID1A* mutation and high CXCL13, and 1.9 months (95% CI, 1.7 to 2.0) in patients with no *ARID1A* mutation and low CXCL13 ($P = 0.02$) (Fig. 3A). We observed a median OS of 19.1 months (95% CI, 6.1 to NA) in patients with *ARID1A* mutation and high CXCL13, 5.7 months (95% CI, 1.5 to 14.0) in patients with *ARID1A* mutation and low CXCL13, 9.5 months (95% CI, 4.5 to 13.5) in patients with no *ARID1A* mutation and high CXCL13, and 5.3 months (95% CI, 3.6 to 11.4) in patients with no *ARID1A* mutation and low CXCL13 (P = ns) (Fig. 3B). In addition, analysis of the hazard curves for CXCL13 by *ARID1A* mutation status suggested that positive association of *ARID1A* mutation with PFS and OS increased in magnitude

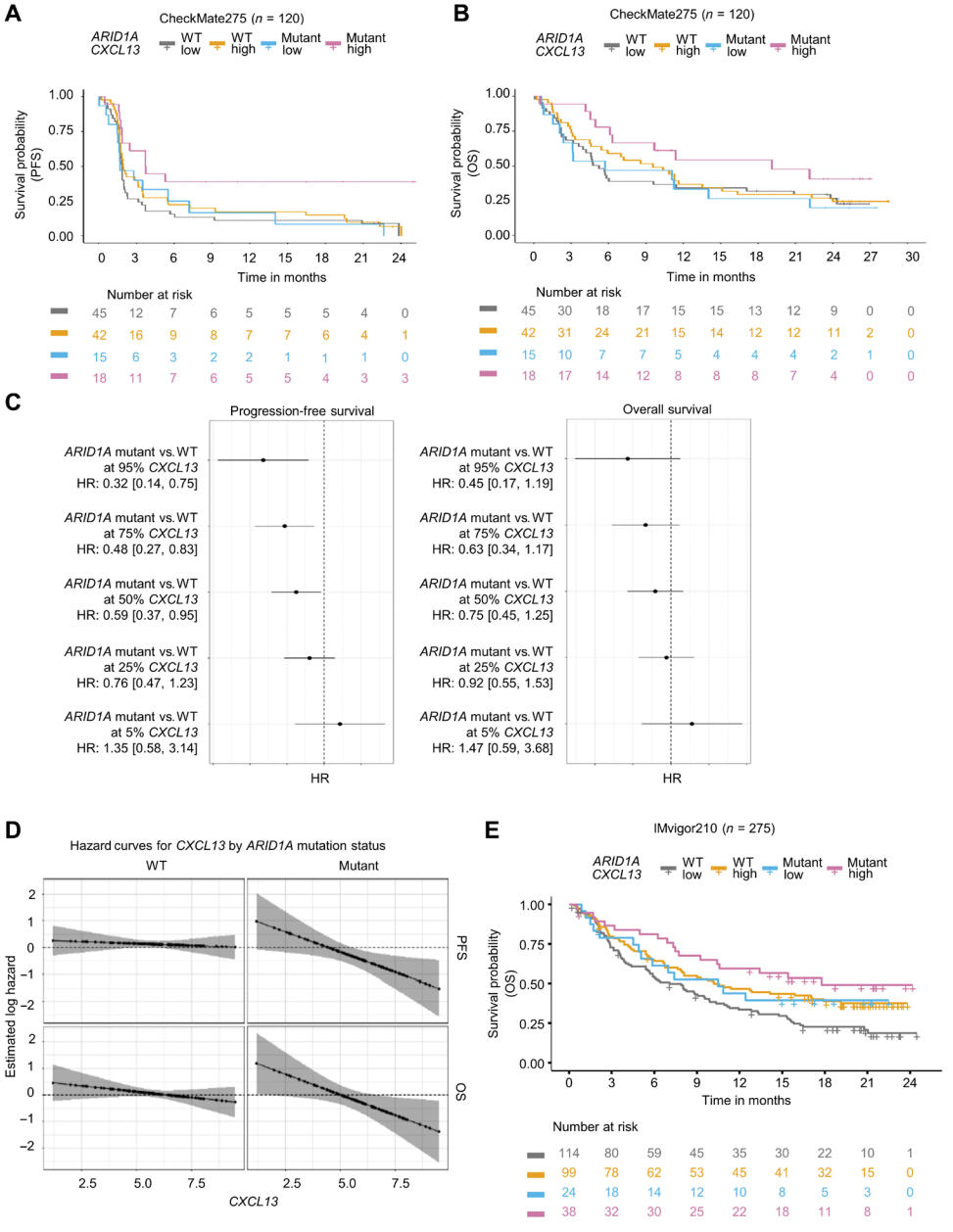

Fig. 3. Combination of *ARID1A* mutation and baseline expression of CXCL13 has improved predictiveness compared to single biomarkers. (**A** and **B**) Kaplan-Meier estimates of PFS ($P = 0.02$) (A) and OS (B) stratified according to *ARID1A* mutation status and 50th percentile of *CXCL13* expression values in the CheckMate275 trial. (**C**) Hazard ratio (HR) estimates for PFS and OS in CheckMate275 subjects. Plotting symbols give point estimates of HR; horizontal bars give 95% CIs. HRs compare *ARID1A* WT and mutant status at different *CXCL13* expression values. (**D**) Predicted log hazard curves demonstrating associations of *CXCL13* expression at different *ARID1A* mutation statuses with PFS and OS. Hazard curve estimates are from the Cox PH model with linear predictors *CXCL13* and *ARID1A* mutation status and *CXCL13*:*ARID1A* mutation status interaction. Shaded areas give 95% pointwise CIs for the hazard curves. Hazard curve estimates were scaled to be zero at the median of *CXCL13* score. (**E**) Kaplan-Meier estimates of OS in patients in the IMvigor210 trial, stratified according to *ARID1A* mutation status and 50th percentile of *CXCL13* expression values ($P = 0.006$).

as CXCL13 gene expression increased (Fig. 3, C and D). The association between CXCL13 expression and response was stronger in patients harboring *ARID1A* mutation compared to patients without *ARID1A* mutation. Further, in IMvigor210, we noted a significant correlation of improved OS with combination of mutation in *ARID1A* plus baseline CXCL13 expression compared to either single biomarker ($P = 0.006$) (Fig. 3E). We observed a median OS of 17.8 months (95% CI, 10.4 to NA) in patients with *ARID1A* mutation and high CXCL13, 10.5 months (95% CI, 5.1 to NA) in patients with *ARID1A* mutation and low CXCL13, 10.2 months (95% CI, 7.9 to 19.1) in patients with no *ARID1A* mutation and high CXCL13, and 7.1 months (95% CI, 5.5 to 9.9) in patients with no *ARID1A* mutation and low CXCL13 (Fig. 3E). Also, similar to CheckMate275, analysis of the hazard curves for CXCL13 by *ARID1A* mutation status showed positive association of *ARID1A* mutation with OS with increase in CXCL13 gene expression (fig. S7). Together, we showed that *ARID1A* mutation plus baseline CXCL13 expression in the tumor tissues may act as a combination biomarker to help select patients with mUCC to receive ICT. Overall, our data suggest that combination biomarker approaches may be more accurate than single biomarkers for predicting clinical responses.

DISCUSSION

It is increasingly clear that immune responses to ICT are influenced by both immune cells and tumor-associated factors. It was demonstrated that in patients with mUCC, high T cell infiltration, which is considered a good predictive marker, is associated with poor clinical outcome of ICT in the presence of a higher epithelial-mesenchymal transition–related stromal gene signature (*25*). Further, stromal cell–derived TGFβ signaling was associated with lack of response to ICT (*16*, *26*), thereby highlighting the interaction of tumors and their immune ecosystem. Therefore, composite biomarkers identified through interrogation of the tumor-immune ecosystem are needed to guide treatment decisions. A recent report showed that patients with high TMB plus high T cell GEP have better responses to ICT than TMB-high or GEP-high signature alone (*27*). GEP was obtained using an 18-gene signature. Although GEP and TMB have been correlated with response to ICT and improved PFS, they will need optimization in terms of GEP calculations in individual patients to incorporate into clinical practice. Further, the sets of genes used to calculate GEP differ markedly in different trials (*5*, *16*, *27*, *28*). In addition, unlike for non–small cell lung cancer, there is no validated

cutoff for TMB in urothelial cancer. Therefore, identification of a single commonly mutated gene in urothelial cancer, as well as baseline expression of a single gene assessed by currently available methods, would have immediate translational potential.

Cancer Genome Atlas Project identified *ARID1A* as one of the recurrent mutations in patients with mUCC (*29*), underscoring the importance of evaluating the impact of *ARID1A* mutation on ICT. *ARID1A* (also known as BAF250a) is a component of the SWI/SNF complex and is a tumor suppressor. *ARID1A* has roles in regulation of the cell cycle, DNA damage checkpoint, P53 targets, and telomerase activity (*30*). A recent study demonstrated that *ARID1A* interacts with mismatch repair protein MutS homolog 2 (MSH2) and regulates mutagenesis, which could be another aspect of its tumor-suppressive role (*19*). Similar to previous reports, we noted that patients harboring *ARID1A* mutations have higher TMB compared to patients without the mutation. In addition, we noted that patients with *ARID1A* mutation also have lower expression of TGFβ1. It was shown that TGFβ1 can attenuate the response to anti–PD-L1 therapy by excluding T cells from the tumor microenvironment (*16*). Collectively, these data suggested that mutation of *ARID1A* can modify the tumor immune microenvironment via multiple pathways, conferring sensitivity to ICT. However, a recent preclinical study showed that aberrations in ARID1A can reduce sensitivity to ICT via an EZH2-mediated pathway (*31*). ARID1A is a chromatin remodeler that interacts with multiple proteins and could affect the function of interacting proteins in a context-dependent manner. Overall, based on our preclinical data and findings from two independent large clinical cohorts, our data demonstrated that *ARID1A* mutation likely confers sensitivity to ICT rather than resistance. Future preclinical and clinical studies should explore how specific *ARID1A* mutations affect the tumor immune microenvironment.

CXCL13 plays a critical role in lymphocyte infiltration as well as TLS formation (*24*). We did not note any difference in CXCL13 expression between *ARID1A*-WT and *ARID1A*-mutant patients, suggesting that *ARID1A* mutation and expression of CXCL13 might not be directly linked, but they may act together to modulate the tumor immune microenvironment, which will need to be evaluated in future studies. Further, this is a retrospective analysis of two clinical trials correlating *ARID1A* mutation, baseline expression of CXCL13, and their combination with OS in patients with mUCC receiving ICT. Combination of the two biomarkers in baseline tumor tissues suggested improved prediction of responses to ICT compared to either single biomarker, which will need to be tested prospectively. Cumulatively, this study provides insight into the importance of linking tumor cell status with immune responses for identification of relevant biomarkers that can predict clinical outcomes for patients receiving ICT and enable patient selection for future clinical trials.

MATERIALS AND METHODS

Study design

The overall objective of this study was to identify predictive combinatorial biomarkers in patients with mUCC receiving ICT to enable better patient selection for ICT. We performed our initial analysis in an MD Anderson discovery cohort (n = 31) using multiple approaches such as whole-exome sequencing, NanoString, and IHC assays. We identified *ARID1A* mutation in the tumor and CXCL13 expression in the baseline tumor tissues as predictors of response to ICT in patients with mUCC. Next, we performed reverse translational studies to gain mechanistic insights into the roles of CXCL13 and *ARID1A*. Murine bladder cancer tumor cell line MB49 was implanted in WT C57BL/6 and CXCL13$^{-/-}$ mice, and tumor-bearing mice were randomized to untreated and anti–PD-1 treatment groups. The tumor growth was assessed, and tumor volumes were measured on day 14 in all groups for antitumor efficacy. Mass cytometry (cytometry by time of flight/CyTOF) and FLOWSOM analysis were performed to phenotype tumor-infiltrating immune cells. We performed RNA-seq of *ARID1A*-knockdown MB49 cells to evaluate pathways affected by ARID1A. The investigators were not blinded to the experimental groups. Next, we confirmed our findings from the discovery cohort and reverse translational studies using two confirmatory cohorts, CheckMate275 (NCT02387996) and IMvigor210 (NCT02108652, NCT02951767). The objective responses were determined on the basis of a blinded independent review committee assessment. In CheckMate275, we used whole-exome sequencing and gene expression data to correlate with response, OS, and PFS. For IMvigor210, we used a publicly available database to correlate responses with *ARID1A* mutation and CXCL13 expression (*16*). Last, we assessed the predictive capability of *ARID1A* mutation and CXCL13 expression as a combinatorial biomarker in our confirmatory cohorts.

Patients and samples

mUCC discovery cohort: Samples were collected as a part of (i) a phase 2 study assessing the safety and efficacy of nivolumab in metastatic or surgically unresectable urothelial carcinoma whose disease progressed or recurred despite previous treatment with at least one platinum-based chemotherapy regimen (NCT02387996) and (ii) a phase 1/2, open-label study of nivolumab monotherapy or nivolumab combined with ipilimumab in subjects with advanced or metastatic solid tumors (NCT01928394). Patient samples were collected after appropriate informed consent was obtained on MD Anderson Institutional Review Board (IRB)–approved protocol PA13-0291.

For the confirmatory cohort, we used The CheckMate275 (NCT02387996) dataset consisting of 270 patients with platinum-resistant mUCC treated with nivolumab on a phase 2 clinical trial that has been described previously (*15*, *25*). The response assessments and survival follow-up of this cohort have previously been described (*15*). Archival formalin-fixed paraffin-embedded (FFPE) mUCC tumor specimens were submitted for each patient before initiation of nivolumab. Gene expression was measured using the HTG EdgeSeq System (HTG Molecular) Oncology and Immuno-Oncology Biomarker Panels. Data were transformed into $\log_2$ trimmed mean of M-values (TMM), normalized counts per million (CPM) before analysis based on the manufacturer's instructions.

IMvigor210 was a single-arm phase 2 study to investigate atezolizumab in patients with mUCC (NCT02108652, NCT02951767). RECIST v1.1 was used to assess response to therapy, as described previously (*3*, *4*). All the data of IMvigor210 trial were accessed through the IMvigor210CoreBiologies R package downloaded from http://research-pub.gene.com/IMvigor210CoreBiologies. The RNA-seq count data were normalized using TMM and transformed with voom to $\log_2$-CPM with associated precision weights as mentioned in a previous publication (*16*).

Mice

C57BL/6 mice (5 to 7 weeks) were purchased from the National Cancer Institute (NCI) (Frederick, MD), and *CXCL13* null (*CXCL13*$^{-/-}$)

mice in the C57BL/6 background (stock no. 005626; 5 to 7 weeks) were purchased from The Jackson Laboratory. All mice were kept in specific pathogen–free conditions in the Animal Resource Center at The University of Texas MD Anderson Cancer Center. Animal protocols were approved by the Institutional Animal Care and Use Committee (IACUC) of The University of Texas MD Anderson Cancer Center.

Cell lines and tumor model

Murine bladder cancer cell line (MB49) was provided by J.P.A. MB49 cells (2×10^5) were injected subcutaneously in the right flank of C57BL/6 mice (5 to 10 mice per group). Anti–PD-1 (clone RMP1-14) antibody was purchased from Bio X Cell. Mice were intraperitoneally injected with anti–PD-1 on days 3 (200 μg per mouse), 6 (100 μg per mouse), and 9 (100 μg per mouse) after tumor inoculation. Tumors were then harvested on day 14 for immune cell analysis.

Whole-exome sequencing data analysis

DNA from FFPE tissues and peripheral blood was obtained using the QIAamp DNA FFPE Tissue Kit and QIAamp DNA Mini Kit, respectively (Qiagen). Whole-exome sequencing experiments were performed on tumor tissues from 68 patients (37 responders and 31 nonresponders). DNA isolated from peripheral blood was used as control. Genomic DNA (250 ng) was sheared using low tris-EDTA buffer. KAPA HyperPrep Kit (#KK8504) was used for end repair, A-base addition, adaptor ligation, and library enrichment polymerase chain reaction. Library construction was performed following the manufacturer's instructions. Sample concentrations were measured after library construction using the Agilent Bioanalyzer. Hybridization reaction and target capture were performed (Agilent SureSelectXT Target Enrichment, #5190-8646) as per the manufacturer's instructions. The libraries were then normalized to equal concentrations using an Eppendorf Mastercycler EP Gradient instrument and pooled to equimolar amounts on the Agilent Bravo B platform. Libraries were quantified using the KAPA Library Quantification Kit (#KK4824). The BWA aligner (bwa-0.7.5a) was applied to map the raw reads to the human hg19 reference genome (UCSC genome browser: genome.ucsc.edu). The average exome-wide coverage ranges were 75.6- to 294.9-fold (median, 182.6) in tumor samples and 47.2- to 140.4-fold (median, 91.56) in the matched normal samples. The Picard (v1.112, http://broadinstitute.github.io/picard/) module "MarkDuplicates" was applied to mark the duplicate reads. Then, the "IndelRealigner" and "BaseRecalibrator" modules of the Genome Analysis Toolkit were applied to perform indel realignment and base quality recalibration. MuTect (v1.1.4) and Pindel (v0.2.4 t) were applied to each tumor and matched normal PBMC sample to detect somatic single-nucleotide variants (SNVs) and small insertions/deletions. To ensure specificity, the following criteria were applied to filter the detected somatic SNVs and indels: The average is at least 20 reads for the tumor and 10 for the normal; the total number of reads supporting the variant is at least 4 and the tumor alternate allele frequency (AF) is at least 5%; the MuTect logarithm of the odds (LOD) score is at least 9.0. To avoid including germline mutations, we further required the AF < 0.01 from the ESP6500, 1000 genome, and EXAC databases. If repetitive sequences were detected within 25 base pairs (bp) in the downstream regions of an indel, that indel was discarded. Only missense, nonsense, and frame-shifting indels in the exonic regions and mutations at splice sites and untranslated regions were included in the downstream analysis. There are 24 samples that passed the quality control (QC) steps with meaningful overall response calls: 11 from responders and 13 from nonresponders. The filtered mutation data were analyzed using the R package maftools (*32*).

TCGA analysis

The RNA-seq expression data of TCGA Bladder Cancer (BLCA) were downloaded from NCI Genomic Data Commons (GDC; https://portal.gdc.cancer.gov). The information on *ARID1A* mutation status and TMB was obtained from the TCGA-BLCA study (*17*), and the relevant clinical outcome data were described by the recent TCGA PanCancer clinical data study (*33*). The normalized RNA-seq expression matrix was transformed as $\log_2$ (FPKM + 1) for downstream analysis.

Mass cytometry (CyTOF)

Freshly collected MB49 tumors from the mice were dissociated with Liberase/deoxyribonuclease (DNase) solution and incubated for 30 min at 37°C, and then single-cell suspensions were made. Around 3 million cells per sample were taken for CyTOF staining. Antibodies were either purchased preconjugated from Fluidigm or purchased purified and conjugated in-house using MaxPar X8 Polymer kits (Fluidigm) according to the manufacturer's instructions (data file S3). Briefly, samples were stained with cell surface antibodies for 30 min at 4°C and then stained for viability with 5 μM cisplatin in 5% fluorescence-activated cell sorting (FACS) buffer for 1 min at room temperature. Samples were then washed, fixed and permeabilized (eBioscience), and stained with intracellular antibodies for 30 min at 4°C. After staining, the samples were washed and barcoded using the manufacturer's protocol (Fluidigm), then incubated with 125 μM Ir intercalator (Fluidigm) in 1.6% paraformaldehyde (PFA)/phosphate-buffered saline (PBS), and stored at 4°C overnight. The cells were then washed with PBS the next day and stored until acquisition. Right before acquisition, samples were washed twice with Milli-Q water, resuspended in water containing EQ 4 element beads (Fluidigm), and run on a Helios mass cytometer (Fluidigm).

Mass cytometry analysis

Files were manually gated in FlowJo by event length for singlets and live/dead discrimination and using CD45 lineage marker for immune cells. Fcs files were then loaded into R using the flowCore package as a flowset for downstream analysis. Data were arcsinh-transformed using a coefficient of 5 (x_transformed = asinh(x/5)). Clustering analysis was performed using the FlowSOM and the ConsensusClusterPlus packages as previously described (*34*). Clusters were identified using PhenoGraph on a per-sample basis in the space formed by these principal components, and cluster frequency plots were generated.

NanoString

RNA was isolated from FFPE tumor sections by dewaxing using deparaffinization solution (Qiagen), and total RNA was extracted using the RecoverAll Total Nucleic Acid Isolation Kit (Ambion) according to the manufacturer's instructions. The RNA purity was assessed on an ND-Nanodrop1000 spectrometer (Thermo Fisher Scientific). For the NanoString platform, 100 ng of RNA was used to detect immune gene expression using nCounter PanCancer Immune Profiling panel along with custom CodeSet (used by NanoString to designate the custom genes included in this study). Counts of the reporter probes were tabulated for each sample by the nCounter Digital Analyzer, and raw data output was imported into nSolver

(www.nanostring.com/products/nSolver). nSolver data analysis package was used for normalization, and hierarchical clustering heatmap analysis was performed with Qlucore Omics Explorer version 3.5 software (Qlucore).

Immunohistochemistry

Hematoxylin and eosin (H&E) and IHC staining was performed on FFPE tumor tissue sections. The tumor tissues were fixed in 10% formalin, embedded in paraffin, and transversely sectioned. Four-micrometer sections were used for the histopathological studies. Sections were stained with mouse or rabbit anti-human monoclonal antibodies against CD3 (Dako, catalog no. A0452), CD4 (Novocastra, CD4-368-L-A), CD8 (Thermo Fisher Scientific, MS-457-S), CD45RO (Novocastra, PA0146), GzmB (Leica Microsystems, PA0291), CD68 (Dako, M0876), and CD20 (DAKO, M0755). All sections were counterstained with H&E, dehydrated, and mounted. All sections were processed with peroxidase-conjugated avidin/biotin and 3′-3-diaminobenzidine (DAB) substrate (Leica Microsystems), and slides were scanned and digitalized using the scanscope system from ScanScope XT, Aperio/Leica Technologies. Quantitative analysis of IHC staining was conducted using the image analysis software ImageScope-Aperio/Leica. Five random areas (1 mm^2 each) were selected using the Aperio Membrane Algorithm and the Aperio Nuclear Algorithm (www.leicabiosystems.com/digital-pathology/analyze/ihc/) for each marker to determine the number of positive cells at high-power field. The data are expressed as a density (total number of positive cells/mm^2 area). IHC staining was interpreted in conjunction with H&E-stained sections.

Multiplex immunofluorescence assay and analysis

For multiplex immunofluorescence staining, the Opal protocol staining method (*35*) was used, and the slides were stained and analyzed for the following markers: CD20 (Dako, catalog no. M0755) with subsequent visualization using fluorescein Cy5, CD4 (CM153BK, Biocare) with subsequent visualization using fluorescein Cy3, and CD8 (M7103, Dako) with subsequent visualization using fluorescein Cy5.5, and nuclei were visualized with 4′,6-diamidino-2-phenylindole (DAPI). All of the sections were mounted using VECTASHIELD HardSet 895 mounting medium.

Slides were scanned using a Vectra slide scanner (PerkinElmer). For each marker, the mean fluorescent intensity per case was then determined as a base point from which positive calls could be established. For multispectral analysis, each of the individually stained sections was used to establish the spectral library of the fluorophores. Five random areas on each sample were analyzed.

TLS quantification

TLSs were qualified and quantified using both H&E and CD20 IHC staining. Structures were identified as aggregates of lymphocytes having histologic features with analogous structures to those of lymphoid tissue with follicles, appearing in the tumor area. For the current study, criteria used for the quantification of TLSs included (i) the total number of structures identified either within the tumoral area or in direct contact with the tumoral cells on the margin of the tumors (numbers of TLSs/1 mm^2 area) and (ii) a normalization of the total area occupied by the TLSs in relation to the total area of the tumor analyzed (ratio: area of TLSs/area of tumor + TLSs).

Statistics

Cox proportional hazards (PH) regression models were used to assess the dependence of OS on gene expression score. PH assumptions were assessed by examination of scaled Schoenfeld residuals. For all Cox PH models, the PH assumption appeared reasonable. The magnitudes of associations were summarized by hazard ratios (HRs). Reported HRs were scaled to *z* score of the biomarker scores. Because the effects of the biomarkers were constrained to be linear in these models, the HR estimates depended only on SD of the gene expression score, not on the individual values. Two-sided 95% CIs for HRs were based on Wald test statistics. Kaplan-Meier plots based on categorization of the biomarker scores were used to illustrate associations with OS. The magnitudes of associations were summarized by odds ratios (ORs), scaled in the same way as the reported HRs. Two-sided 95% CIs for ORs were based on Wald test statistics. Two-sided 95% CIs for objective response rate were estimated by the Clopper-Pearson exact method. Likelihood ratio tests were used to test overall biomarker effects. Kaplan-Meier plots based on categorization of the biomarker scores were used to illustrate associations with OS. All data analyses were performed with R 3.4.1 for Linux and R 3.5.2 for Windows.

For murine experiments, all data are representative of at least two to three independent experiments with 5 to 10 mice in each in vivo experiment. The data are expressed as mean ± SEM and were analyzed using Prism 7.0 statistical analysis software (GraphPad Software). Student's *t* tests (two-tailed), analysis of variance (ANOVA), and Bonferroni multiple-comparison tests were used to identify significant differences ($P < 0.05$) between treatment groups.

SUPPLEMENTARY MATERIALS

stm.sciencemag.org/cgi/content/full/12/548/eabc4220/DC1

Fig. S1. CONSORT diagram for CheckMate275 and IMvigor210.

Fig. S2. Loss of *ARID1A* enhances the immunogenicity of bladder tumor cells.

Fig. S3. Patients harboring *ARID1A* gene mutation have higher TMB.

Fig. S4. Analysis of *TGFβ1* and PD-L1 expression in patients with and without *ARID1A* mutations.

Fig. S5. TLS in baseline tumor tissues correlated with improved response in the discovery cohort.

Fig. S6. *CXCL13*$^{-/-}$ mice are resistant to anti–PD-1 therapy.

Fig. S7. Combination of *ARID1A* mutation and baseline expression of *CXCL13* in the tumor tissue predicts performance of ICT.

Data file S1. Patient characteristics with correlative assays performed.

Data file S2. Expression data of NanoString Gene Panel.

Data file S3. Antibodies used for murine CyTOF analysis.

View/request a protocol for this paper from *Bio-protocol*.

REFERENCES AND NOTES

1. R. L. Siegel, K. D. Miller, A. Jemal, Cancer statistics, 2020. *CA Cancer J. Clin.* **70**, 7–30 (2020).
2. T. Powles, J. P. Eder, G. D. Fine, F. S. Braiteh, Y. Loriot, C. Cruz, J. Bellmunt, H. A. Burris, D. P. Petrylak, S. L. Teng, X. Shen, Z. Boyd, P. S. Hegde, D. S. Chen, N. J. Vogelzang, MPDL3280A (anti-PD-L1) treatment leads to clinical activity in metastatic bladder cancer. *Nature* **515**, 558–562 (2014).
3. J. E. Rosenberg, J. Hoffman-Censits, T. Powles, M. S. van der Heijden, A. V. Balar, A. Necchi, N. Dawson, P. H. O'Donnell, A. Balmanoukian, Y. Loriot, S. Srinivas, M. M. Retz, P. Grivas, R. W. Joseph, M. D. Galsky, M. T. Fleming, D. P. Petrylak, J. L. Perez-Gracia, H. A. Burris, D. Castellano, C. Canil, J. Bellmunt, D. Bajorin, D. Nickles, R. Bourgon, G. M. Frampton, N. Cui, S. Mariathasan, O. Abidoye, G. D. Fine, R. Dreicer, Atezolizumab in patients with locally advanced and metastatic urothelial carcinoma who have progressed following treatment with platinum-based chemotherapy: A single-arm, multicentre, phase 2 trial. *Lancet* **387**, 1909–1920 (2016).
4. A. V. Balar, M. D. Galsky, J. E. Rosenberg, T. Powles, D. P. Petrylak, J. Bellmunt, Y. Loriot, A. Necchi, J. Hoffman-Censits, J. L. Perez-Gracia, N. A. Dawson, M. S. van der Heijden, R. Dreicer, S. Srinivas, M. M. Retz, R. W. Joseph, A. Drakaki, U. N. Vaishampayan, S. S. Sridhar, D. I. Quinn, I. Duran, D. R. Shaffer, B. J. Eigl, P. D. Grivas, E. Y. Yu, S. Li, E. E. Kadel III, Z. Boyd, R. Bourgon, P. S. Hegde, S. Mariathasan, A. Thåström, O. O. Abidoye, G. D. Fine, D. F. Bajorin; IMvigor210 Study Group, Atezolizumab as first-line treatment in cisplatin-ineligible patients with locally advanced and metastatic urothelial carcinoma: A single-arm, multicentre, phase 2 trial. *Lancet* **389**, 67–76 (2017).

5. P. Sharma, M. Retz, A. Siefker-Radtke, A. Baron, A. Necchi, J. Bedke, E. R. Plimack, D. Vaena, M.-O. Grimm, S. Bracarda, J. Á. Arranz, S. Pal, C. Ohyama, A. Saci, X. Qu, A. Lambert, S. Krishnan, A. Azrilevich, M. D. Galsky, Nivolumab in metastatic urothelial carcinoma after platinum therapy (CheckMate 275): A multicentre, single-arm, phase 2 trial. *Lancet Oncol.* **18**, 312–322 (2017).
6. J. Bellmunt, R. de Wit, D. J. Vaughn, Y. Fradet, J.-L. Lee, L. Fong, N. J. Vogelzang, M. A. Climent, D. P. Petrylak, T. K. Choueiri, A. Necchi, W. Gerritsen, H. Gurney, D. I. Quinn, S. Culine, C. N. Sternberg, Y. Mai, C. H. Poehlein, R. F. Perini, D. F. Bajorin; KEYNOTE-045 Investigators, Pembrolizumab as second-line therapy for advanced urothelial carcinoma. *N. Engl. J. Med.* **376**, 1015–1026 (2017).
7. C. Massard, M. S. Gordon, S. Sharma, S. Rafii, Z. A. Wainberg, J. Luke, T. J. Curiel, G. Colon-Otero, O. Hamid, R. E. Sanborn, P. H. O'Donnell, A. Drakaki, W. Tan, J. F. Kurland, M. C. Rebelatto, X. Jin, J. A. Blake-Haskins, A. Gupta, N. H. Segal, Safety and efficacy of durvalumab (MEDI4736), an anti-programmed cell death ligand-1 immune checkpoint inhibitor, in patients with advanced urothelial bladder cancer. *J. Clin. Oncol.* **34**, 3119–3125 (2016).
8. C. G. Drake, T. J. Bivalacqua, N. M. Hahn, Programmed cell death ligand-1 blockade in urothelial bladder cancer: To select or not to select. *J. Clin. Oncol.* **34**, 3115–3116 (2016).
9. A. B. Apolo, J. R. Infante, A. Balmanoukian, M. R. Patel, D. Wang, K. Kelly, A. E. Mega, C. D. Britten, A. Ravaud, A. C. Mita, H. Safran, T. E. Stinchcombe, M. Srdanov, A. B. Gelb, M. Schlichting, K. Chin, J. L. Gulley, Avelumab, an anti-programmed death-ligand 1 antibody, in patients with refractory metastatic urothelial carcinoma: Results from a multicenter, phase Ib study. *J. Clin. Oncol.* **35**, 2117–2124 (2017).
10. D. Gopalakrishnan, V. S. Koshkin, M. C. Ornstein, A. Papatsoris, P. Grivas, Immune checkpoint inhibitors in urothelial cancer: Recent updates and future outlook. *Ther. Clin. Risk Manag.* **14**, 1019–1040 (2018).
11. D. H. Aggen, C. G. Drake, Biomarkers for immunotherapy in bladder cancer: A moving target. *J. Immunother. Cancer* **5**, 94 (2017).
12. P. Sharma, Immune checkpoint therapy and the search for predictive biomarkers. *Cancer J.* **22**, 68–72 (2016).
13. A. A. Davis, V. G. Patel, The role of PD-L1 expression as a predictive biomarker: An analysis of all US Food and Drug Administration (FDA) approvals of immune checkpoint inhibitors. *J. Immunother. Cancer* **7**, 278 (2019).
14. J.-M. Lavoie, P. C. Black, B. J. Eigl, Predictive biomarkers for checkpoint blockade in urothelial cancer: A systematic review. *J. Urol.* **202**, 49–56 (2019).
15. P. Sharma, M. K. Callahan, P. Bono, J. Kim, P. Spiliopoulou, E. Calvo, R. N. Pillai, P. A. Ott, F. de Braud, M. Morse, D. T. Le, D. Jaeger, E. Chan, C. Harbison, C.-S. Lin, M. Tschaika, A. Azrilevich, J. E. Rosenberg, Nivolumab monotherapy in recurrent metastatic urothelial carcinoma (CheckMate 032): A multicentre, open-label, two-stage, multi-arm, phase 1/2 trial. *Lancet Oncol.* **17**, 1590–1598 (2016).
16. S. Mariathasan, S. J. Turley, D. Nickles, A. Castiglioni, K. Yuen, Y. Wang, E. E. Kadel III, H. Koeppen, J. L. Astarita, R. Cubas, S. Jhunjhunwala, R. Banchereau, Y. Yang, Y. Guan, C. Chalouni, J. Ziai, Y. Şenbabaoğlu, S. Santoro, D. Sheinson, J. Hung, J. M. Giltnane, A. A. Pierce, K. Mesh, S. Lianoglou, J. Riegler, R. A. D. Carano, P. Eriksson, M. Höglund, L. Somarriba, D. L. Halligan, M. S. van der Heijden, Y. Loriot, J. E. Rosenberg, L. Fong, I. Mellman, D. S. Chen, M. Green, C. Derleth, G. D. Fine, P. S. Hegde, R. Bourgon, T. Powles, TGFβ attenuates tumour response to PD-L1 blockade by contributing to exclusion of T cells. *Nature* **554**, 544–548 (2018).
17. A. G. Robertson, J. Kim, H. Al-Ahmadie, J. Bellmunt, G. Guo, A. D. Cherniack, T. Hinoue, P. W. Laird, K. A. Hoadley, R. Akbani, M. A. A. Castro, E. A. Gibb, R. S. Kanchi, D. A. Gordenin, S. A. Shukla, F. Sanchez-Vega, D. E. Hansel, B. A. Czerniak, V. E. Reuter, X. Su, B. de Sa Carvalho, V. S. Chagas, K. L. Mungall, S. Sadeghi, C. S. Pedamallu, Y. Lu, L. J. Klimczak, J. Zhang, C. Choo, A. I. Ojesina, S. Bullman, K. M. Leraas, T. M. Lichtenberg, C. J. Wu, N. Schultz, G. Getz, M. Meyerson, G. B. Mills, D. J. McConkey; TCGA Research Network, J. N. Weinstein, D. J. Kwiatkowski, S. P. Lerner, Comprehensive molecular characterization of muscle-invasive bladder cancer. *Cell* **171**, 540–556.e25 (2017).
18. X. Wang, N. G. Nagl Jr., S. Flowers, D. Zweitzig, P. B. Dallas, E. Moran, Expression of p270 (ARID1A), a component of human SWI/SNF complexes, in human tumors. *Int. J. Cancer* **112**, 636 (2004).
19. J. Shen, Z. Ju, W. Zhao, L. Wang, Y. Peng, Z. Ge, Z. D. Nagel, J. Zou, C. Wang, P. Kapoor, X. Ma, D. Ma, J. Liang, S. Song, J. Liu, L. D. Samson, J. A. Ajani, G.-M. Li, H. Liang, X. Shen, G. B. Mills, G. Peng, ARID1A deficiency promotes mutability and potentiates therapeutic antitumor immunity unleashed by immune checkpoint blockade. *Nat. Med.* **24**, 556–562 (2018).
20. R. Cabrita, M. Lauss, A. Sanna, M. Donia, M. Skaarup Larsen, S. Mitra, I. Johansson, B. Phung, K. Harbst, J. Vallon-Christersson, A. van Schoiack, K. Lövgren, S. Warren, K. Jirström, H. Olsson, K. Pietras, C. Ingvar, K. Isaksson, D. Schadendorf, H. Schmidt, L. Bastholt, A. Carneiro, J. A. Wargo, I. M. Svane, G. Jönsson, Tertiary lymphoid structures improve immunotherapy and survival in melanoma. *Nature* **577**, 561–565 (2020).
21. B. A. Helmink, S. M. Reddy, J. Gao, S. Zhang, R. Basar, R. Thakur, K. Yizhak, M. Sade-Feldman, J. Blando, G. Han, V. Gopalakrishnan, Y. Xi, H. Zhao, R. N. Amaria, H. A. Tawbi, A. P. Cogdill, W. Liu, V. S. LeBleu, F. G. Kugeratski, S. Patel, M. A. Davies, P. Hwu, J. E. Lee, J. E. Gershenwald, A. Lucci, R. Arora, S. Woodman, E. Z. Keung, P.-O. Gaudreau, A. Reuben, C. N. Spencer, E. M. Burton, L. E. Haydu, A. J. Lazar, R. Zapassodi, C. W. Hudgens, D. A. Ledesma, S. Ong, M. Bailey, S. Warren, D. Rao, O. Krijgsman, E. A. Rozeman, D. Peeper, C. U. Blank, T. N. Schumacher, L. H. Butterfield, M. A. Zelazowska, K. M. McBride, R. Kalluri, J. Allison, F. Petitprez, W. H. Fridman, C. Sautès-Fridman, N. Hacohen, K. Rezvani, P. Sharma, M. T. Tetzlaff, L. Wang, J. A. Wargo, B cells and tertiary lymphoid structures promote immunotherapy response. *Nature* **577**, 549–555 (2020).
22. F. Petitprez, A. de Reyniès, E. Z. Keung, T. W.-W. Chen, C.-M. Sun, J. Calderaro, Y.-M. Jeng, L.-P. Hsiao, L. Lacroix, A. Bougoüin, M. Moreira, G. Lacroix, I. Natario, J. Adam, C. Lucchesi, Y. Laizet, M. Toulmonde, M. A. Burgess, V. Bolejack, D. Reinke, K. M. Wani, W.-L. Wang, A. J. Lazar, C. L. Roland, J. A. Wargo, A. Italiano, C. Sautès-Fridman, H. A. Tawbi, W. H. Fridman, B cells are associated with survival and immunotherapy response in sarcoma. *Nature* **577**, 556–560 (2020).
23. J. L. Messina, D. A. Fenstermacher, S. Eschrich, X. Qu, A. E. Berglund, M. C. Lloyd, M. J. Schell, V. K. Sondak, J. S. Weber, J. J. Mulé, 12-Chemokine gene signature identifies lymph node-like structures in melanoma: Potential for patient selection for immunotherapy? *Sci. Rep.* **2**, 765 (2012).
24. C. Sautès-Fridman, F. Petitprez, J. Calderaro, W. H. Fridman, Tertiary lymphoid structures in the era of cancer immunotherapy. *Nat. Rev. Cancer* **19**, 307–325 (2019).
25. L. Wang, A. Saci, P. M. Szabo, S. D. Chasalow, M. Castillo-Martin, J. Domingo-Domenech, A. Siefker-Radtke, P. Sharma, J. P. Sfakianos, Y. Gong, A. Dominguez-Andres, W. K. Oh, D. Mulholland, A. Azrilevich, L. Hu, C. Cordon-Cardo, H. Salmon, N. Bhardwaj, J. Zhu, M. D. Galsky, EMT- and stroma-related gene expression and resistance to PD-1 blockade in urothelial cancer. *Nat. Commun.* **9**, 3503 (2018).
26. T. Powles, M. Kockx, A. Rodriguez-Vida, I. Duran, S. J. Crabb, M. S. Van Der Heijden, B. Szabados, A. F. Pous, G. Gravis, U. A. Herranz, A. Protheroe, A. Ravaud, D. Maillet, M. J. Mendez, C. Suarez, M. Linch, A. Prendergast, P.-J. van Dam, D. Stanoeva, S. Daelemans, S. Mariathasan, J. S. Tea, K. Mousa, R. Banchereau, D. Castellano, Clinical efficacy and biomarker analysis of neoadjuvant atezolizumab in operable urothelial carcinoma in the ABACUS trial. *Nat. Med.* **25**, 1706–1714 (2019).
27. R. Cristescu, R. Mogg, M. Ayers, A. Albright, E. Murphy, J. Yearley, X. Sher, X. Q. Liu, H. Lu, M. Nebozhyn, C. Zhang, J. K. Lunceford, A. Joe, J. Cheng, A. L. Webber, N. Ibrahim, E. R. Plimack, P. A. Ott, T. Y. Seiwert, A. Ribas, T. K. McClanahan, J. E. Tomassini, A. Loboda, D. Kaufman, Pan-tumor genomic biomarkers for PD-1 checkpoint blockade-based immunotherapy. *Science* **362**, eaar3593 (2018).
28. M. Ayers, J. Lunceford, M. Nebozhyn, E. Murphy, A. Loboda, D. R. Kaufman, A. Albright, J. D. Cheng, S. P. Kang, V. Shankaran, S. A. Piha-Paul, J. Yearley, T. Y. Seiwert, A. Ribas, T. K. McClanahan, IFN-γ-related mRNA profile predicts clinical response to PD-1 blockade. *J. Clin. Invest.* **127**, 2930–2940 (2017).
29. Cancer Genome Atlas Research Network, Comprehensive molecular characterization of urothelial bladder carcinoma. *Nature* **507**, 315–322 (2014).
30. R. Mathur, ARID1A loss in cancer: Towards a mechanistic understanding. *Pharmacol. Ther.* **190**, 15–23 (2018).
31. J. Li, W. Wang, Y. Zhang, M. Cieslik, J. Guo, M. Tan, M. D. Green, W. Wang, H. Lin, W. Li, S. Wei, J. Zhou, G. Li, X. Jing, L. Vatan, L. Zhao, B. Bitler, R. Zhang, K. R. Cho, Y. Dou, I. Kryczek, T. A. Chan, D. Huntsman, A. M. Chinnaiyan, W. Zou, Epigenetic driver mutations in ARID1A shape cancer immune phenotype and immunotherapy. *J. Clin. Invest.* **130**, 2712–2726 (2020).
32. A. Mayakonda, D.-C. Lin, Y. Assenov, C. Plass, H. P. Koeffler, Maftools: Efficient and comprehensive analysis of somatic variants in cancer. *Genome Res.* **28**, 1747–1756 (2018).
33. J. Liu, T. Lichtenberg, K. A. Hoadley, L. M. Poisson, A. J. Lazar, A. D. Cherniack, A. J. Kovatich, C. C. Benz, D. A. Levine, A. V. Lee, L. Omberg, D. M. Wolf, C. D. Shriver, V. Thorsson; Cancer Genome Atlas Research Network, H. Hu, An integrated TCGA pan-cancer clinical data resource to drive high-quality survival outcome analytics. *Cell* **173**, 400–416.e11 (2018).
34. M. Nowicka, C. Krieg, L. M. Weber, F. J. Hartmann, S. Guglietta, B. Becher, M. P. Levesque, M. D. Robinson, CyTOF workflow: Differential discovery in high-throughput high-dimensional cytometry datasets. *F1000Res* **6**, 748 (2017).
35. E. C. Stack, C. Wang, K. A. Roman, C. C. Hoyt, Multiplexed immunohistochemistry, imaging, and quantitation: A review, with an assessment of Tyramide signal amplification, multispectral imaging and multiplex analysis. *Methods* **70**, 46–58 (2014).

Acknowledgments: We would like to acknowledge the Immunotherapy Platform team at MD Anderson Cancer Center for help in obtaining patient samples and processing for immunofluorescence and gene expression analysis. P.S. is a member of the Parker Institute for Cancer Immunotherapy (PICI), and J.P.A. and P.S. are co-directors of the Parker Institute for Cancer Immunotherapy at MD Anderson Cancer Center. S.G. is a PICI physician-scientist, Khalifa, and K12 Calabresi scholar. **Funding:** Parker Institute of Cancer Immunotherapy (P.S.).
Author contributions: P.S. supervised and oversaw the study and acquired the funding. S.G. designed the experiments, analyzed data, and wrote the manuscript. Y.C. and P.M.S. performed statistical analyses. S.A., S.M.N., J.Z., L.X., and B.G. performed the experiments. S.B.,

J.M.B., W.L., and S.S.Y. analyzed the data from the discovery cohort. P.S., S.G., and Y.C. reviewed and edited the text. M.D.G., A.S., and J.P.A. analyzed and interpreted the data. **Competing interests:** J.P.A., P.S., and S.G. have filed a pending provisional patent application entitled "Methods for treating bladder cancer" based on the work in this manuscript. P.S. reports consulting, advisory roles, and/or stocks/ownership for Achelois, Apricity Health, BioAlta, Codiak BioSciences, Constellation, Dragonfly Therapeutics, Forty-Seven Inc., Hummingbird, ImaginAb, Jounce Therapeutics, Lava Therapeutics, Lytix Biopharma, Marker Therapeutics, Neon Therapeutics, Oncolytics, and Polaris and owns a patent licensed to Jounce Therapeutics. J.P.A. reports consulting, advisory roles, and/or stocks/ownership for Achelois, Apricity Health, BioAlta, Codiak BioSciences, Dragonfly Therapeutics, Forty-Seven Inc., Hummingbird, ImaginAb, Jounce Therapeutics, Lava Therapeutics, Lytix Biopharma, Marker Therapeutics, Neon Therapeutics, Polaris, and Tvardi Therapeutics and owns a patent licensed to Jounce Therapeutics. M.D.G. reports consultancy in BioMotiv, Janssen, Astellas, Pfizer, EMD Serono, Seattle Genetics, Inctye, Dracen, Inovio, Aileron, and Dragonfly and grants from Dendreon, Novartis, Merck, Genentech, Bristol Myers Squibb, and AstraZeneca. **Data and materials availability:** The dataset generated during the current study has been uploaded to European Genome Archive (EGA), and accession number is EGAS00001004457. All other data associated with this study are present in the paper or the Supplementary Materials.

Submitted 23 April 2020
Accepted 29 May 2020
Published 17 June 2020
10.1126/scitranslmed.abc4220

Citation: S. Goswami, Y. Chen, S. Anandhan, P. M. Szabo, S. Basu, J. M. Blando, W. Liu, J. Zhang, S. M. Natarajan, L. Xiong, B. Guan, S. S. Yadav, A. Saci, J. P. Allison, M. D. Galsky, P. Sharma, *ARID1A* mutation plus CXCL13 expression act as combinatorial biomarkers to predict responses to immune checkpoint therapy in mUCC. *Sci. Transl. Med.* **12**, eabc4220 (2020).

Science Translational Medicine

ARID1A mutation plus CXCL13 expression act as combinatorial biomarkers to predict responses to immune checkpoint therapy in mUCC

Sangeeta Goswami, Yulong Chen, Swetha Anandhan, Peter M. Szabo, Sreyashi Basu, Jorge M. Blando, Wenbin Liu, Jan Zhang, Seanu Meena Natarajan, Liangwen Xiong, Baoxiang Guan, Shalini Singh Yadav, Abdel Saci, James P. Allison, Matthew D. Galsky and Padmanee Sharma

Sci Transl Med **12**, eabc4220.
DOI: 10.1126/scitranslmed.abc4220

Two markers can be better than one

Therapies targeting immune checkpoints in cancer are achieving increasing prominence because they can achieve long-lasting responses in patients with difficult-to-treat tumors. Unfortunately, not all tumors respond to these treatments, and it is not clear how to identify patients most likely to benefit. Previous studies have suggested individual biomarkers, such as expression of the immune checkpoints themselves, but this was not sufficient. To address this problem, Goswami *et al*. investigated potential biomarker combinations and identified a genetic change and an immune marker, which together helped predict response to immune checkpoint therapy in multiple cohorts of patients with metastatic urothelial carcinoma.